15TH IEA HEAT PUMP CONFERENCE
MAY 26–29, 2026 | HOFBURG
VIENNA 2026
DECARBONISATION THROUGH INNOVATION

Latent heat thermal energy storage performance maps enabling fast & accurate building energy simulations

Mylena Menezes[a], Al-Hussain Othman[a], James Tancabel[a], Vikrant Aute[a*]

[a]Department of Mechanical Engineering, University of Maryland, College Park, MD 20742, United States

Abstract

Thermal energy storage (TES) using phase change materials (PCMs) has gained attention as an effective approach to manage energy demand fluctuations and shift peak building loads. PCM embedded heat exchangers (PCM-HXs) offer high energy storage density and low temperature variation during phase change, being suitable for load-shifting applications. However, this component is typically evaluated using computationally expensive methods, which present significant challenges when the ultimate goal is to assess the performance of PCM-HX integrated thermal energy storage systems in the full building context. In this paper, we present a methodology to generate highly accurate and computationally efficient PCM-HX performance maps which can be easily integrated into building energy simulation tools to analyze the feasibility of space conditioning systems with latent heat PCM-based TES. The performance maps are generated using a computationally efficient PCM-HX simulation tool based on a Generalized Resistance-Capacitance Model (GRCM) which can simulate arbitrary PCM-HXs with high accuracy and significantly less computational effort compared to full CFD simulations. The methodology was verified for a case study considering a 5-ton (~17.5 kW) air-to-water heat pump-thermal energy storage system (HP-TES), which was co-simulated in Modelica for a DOE prototype small-office building in Vienna, Austria, using Spawn of EnergyPlus™. The TES performance maps provided accurate predictions of PCM-HX behavior when used as Modelica component, with deviations within 2-4% while also achieving at least 10^3 computational time reduction. Leveraging this faster prediction capability, four PCMs with different melting temperatures for cooling (12°C, 16°C) and heating (31°C, 36°C) were assessed to investigate their impact on system performance. This work highlights the importance of robust PCM-HX models for efficient and high-fidelity building-level simulations, presenting new opportunities for advanced control strategy development and parametric analysis of TES configurations in a computationally efficient manner.

Selection and/or peer-review under the responsibility of the organizers of the 15th IEA Heat Pump Conference 2026.

Keywords: Spawn of EnergyPlus; Modelica Building Simulations; Performance Maps; Phase Change Material; Resistance-Capacitance Model; Thermal Energy Storage

1. Introduction

Heat pumps (HP) have seen growing interest over the past years due to their potential to support decarbonization, reducing the reliance on conventional fossil fuel-based systems and facilitating the integration of renewable energy generation [1]. In 2024, the total number of heat pumps installed in Europe reached 25.5 million and is projected to triple by 2030 [2]. However, as electrification expands and renewable energy penetration rises the resulting strain on the power grid and rising peak loads present significant challenges [3]. Thermal energy storage (TES) using phase change material (PCM) integrated with HP serves as an effective solution to mitigate these issues by storing surplus energy and smoothing power fluctuations [4], [5]. HP-TES systems incorporating PCMs are gaining attention due to their high latent heat of fusion, which enables efficient thermal energy storage for power supply [6].

However, modelling PCM-TES systems usually requires computationally expensive methods to accurately predict the PCM melting and solidification processes, such as Computational Fluid Dynamics (CFD). Resistance-Capacitance Models (RCMs) have been developed to overcome the computational burden of CFD-

* Corresponding author. *E-mail address:* vikrant@umd.edu

based models by simplifying the PCM-HX domain as a network of thermal resistances and capacitance, analogous an electric circuit, offering a balance between accuracy and computational efficiency [7], [8], [9].

Despite the continued growth of RCMs for PCM-HX thermal performance evaluation, their application in assessing active PCM–TES integration within building-level simulation platforms remains limited. Kamal et al. [10] evaluated a HP-TES system using the EnergyPlus™ built-in TES model with ice as the storage medium to avoid the complexity of detailed PCM-HX simulations. The development of performance maps, as implemented in EnergyPlus™, offers flexibility and simplicity by expanding the range of scenarios where such component models can be effectively applied [11]. RCM map-based models enable rapid prediction of discharge and recharge behavior, supporting broader application of PCM-HX for TES in transient simulations. However, such map-based models cannot be directly implemented in EnergyPlus™ due to the software's pre-defined control strategy, which are primarily for ice storage systems [12].

In this paper, we propose a new methodology for accurate and computationally efficient simulation of building energy systems integrated with PCM-TES. TES map-based models are developed using a Generalized Resistance-Capacitance Model (GRCM) [9], which can accurately predict PCM-HX performance in a computationally efficient manner. A 5-ton (~17.5 kW) air-to-water HP integrated with PCM-based TES is designed to meet both cooling and heating demands of a DOE prototype small-office building [13] and is implemented as a custom component in EnergyPlus™ through Spawn. Simulations were carried out in Vienna, Austria, using IWEC-TMY weather data [14], to demonstrate the feasibility of the methodology.

2. Methodology

The PCM-HX integration with HP leverages the predictive capabilities of the GRCM [9] to simulate PCM-HX thermal performance, enabling its implementation in Modelica. The Spawn of EnergyPlus™ [15] is used to bridge the separate domains of PCM-TES, building simulation, and controls implementation. The Modelica Buildings Library [15], [16] was used to construct the building model (e.g., thermal zones) and supervisory control logic (e.g., switches, Boolean operations, logic gates). Based on design-day building loads, the PCM-HX was sized for the target HP-TES application using GRCM. The resulting outputs were used to generate curve-fitted performance maps of TES behavior, which were subsequently embedded into the Modelica simulations to represent the PCM-HX component within the HP-TES. In parallel, building loads were computed using Spawn of EnergyPlus™ [15], with Dymola [17] providing the dynamic simulation environment coupling EnergyPlus™, the PCM-HX performance maps, HVAC operation and rule-based control (Figure 1).

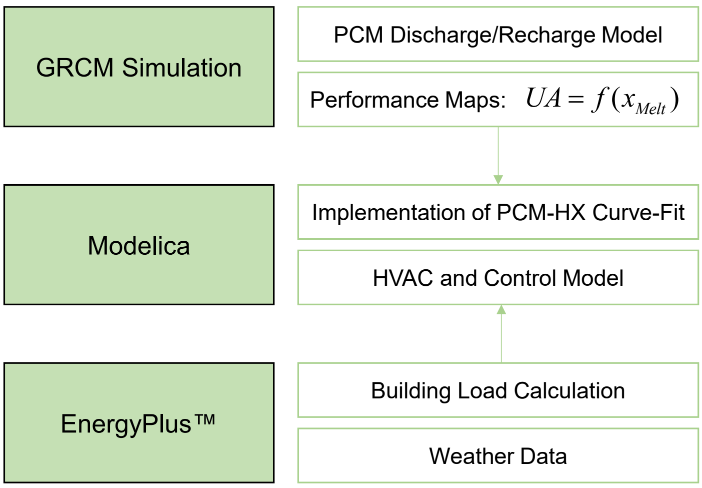

Figure 1. HP-TES building energy simulation workflow

The PCM-HX represents the TES component in the HP-TES integration and were sized to meet the space conditioning load for a DOE small office building [13] for three hours under cooling and heating condition, determined based on a design day conditions specified according to ASHRAE Standard 90.1-2022 [18]. The PCM storage capacity was determined using Eq. (1), where the maximum required discharge rate is for the cooling mode based on the maximum cooling capacity from AHRI 210/240 [19] A-test operating conditions.

$$\boldsymbol{V_{PCM}} = \frac{\int_{t_i}^{t_f} \dot{\boldsymbol{Q}} \boldsymbol{dt}}{\boldsymbol{\rho_{PCM} H_{latent}}} \tag{1}$$

Organic PCMs A31, A36, A12 and A16 [20] were used for heating and cooling modes, respectively, with thermophysical properties as shown in Table 1. For each PCM, a temperature glide of ±2 K is assumed, i.e., fully charged (SOC = 1, fully liquid PCM) occurs at $T = T_{nominal} + 2$ K and fully discharged state (SOC = 0, fully solid PCM) occurs at $T = T_{nominal} - 2$ K.

Table 1. PCM thermophysical properties

Property	Unit	A31 [20]	A36 [20]	A12 [20]	A16 [20]
k (Solid & Liquid)	W/mK	0.21	0.22	0.22	0.18
c_p (Solid & Liquid)	kJ/kgK	2.22	2.3	2.16	2.16
Latent Heat	kJ/kg	230	250	215	225
ρ (Solid & Liquid)	kg/m³	790	776	775	780
Nominal Melting Temperature (Melting Temperature Range)	°C	31 (29-33)	36 (34-38)	12 (10-14)	16 (14-18)

2.1. Thermal Energy Storage Level Performance Maps

An experimentally-validated Generalized Resistance-Capacitance Model (GRCM) that enables high-fidelity, low computational cost predictions of the arbitrary PCM-HX performance was utilized to generate the source data used to construct the performance maps considered herein [9]. The GRCM assumptions include:

- Conduction is the dominant heat transfer mode and natural convection effects are neglected;
- Constant PCM thermophysical properties throughout the domain;
- Adiabatic TES container walls

When using EnergyPlus™, the discharging and recharging performance of TES is modelled using polynomial expressions that correlates different parameters in the unit. King and Potter [21] first developed the polynomial fits for ice-on-coil melting in EnergyPlus™ based on liquid fraction (x_{melt}) and log mean temperature difference (LMTD) between the brine and the storage freezing temperature, as shown in Eq. (**2**).

$$\boldsymbol{UA_{ice}} = \left(\boldsymbol{C_1} + \boldsymbol{C_2 x_{melt}} + \boldsymbol{C_3 x_{melt}^2} + \boldsymbol{C_4 x_{melt}^3} + \boldsymbol{C_5 x_{melt}^4} + \boldsymbol{C_6 x_{melt}^5}\right)\boldsymbol{Q_{stor}}/\boldsymbol{\Delta t} \,/\boldsymbol{LMTD} \tag{2}$$

In this work, the polynomial expression for predicting the thermal behavior are based on the UA values obtained from GRCM, following a similar logic to the empirical formulations used in EnergyPlus™ ice storage model [21], [22], but generalized for any PCM with temperature glide. For the performance maps, the *UA* is modelled as a function of liquid fraction (x_{melt}) only (Eq. (**3**)), dynamically reflecting the changes in behavior during the phase change process. Separate sets of coefficients are generated for discharge and recharge.

$$\boldsymbol{UA_{CF}} = \boldsymbol{C_1} + \boldsymbol{C_2 x_{melt}} + \boldsymbol{C_3 x_{melt}^2} + \boldsymbol{C_4 x_{melt}^3} + \boldsymbol{C_5 x_{melt}^4} + \boldsymbol{C_6 x_{melt}^5} \tag{3}$$

The UA_{CF} coefficients C_i are determined using linear regression, where the liquid fraction x_{melt} and UA_{CF} outputs from the GRCM at each time step serve as source data to the curve-fitting process.

2.2. Case Study: Building Simulation with HP-TES

The 5-ton (~17.5 kW) air-to-water HP system-level performance maps were developed based on transient component and system models using an in-house Modelica library [23]. Additional model details can be found in Qiao et al. [23] and Othman et al. [24], [25]. The HP-TES employs two separate PCM-HXs, one for cooling and one for heating, allowing for the selection of PCM nominal temperatures that are well aligned with outdoor conditions for each season. The schematic of the HP-TES for heating and cooling applications is shown in Figure 2, illustrating base operation (Figure 2a), TES discharge (Figure 2b), and recharge (Figure 2c). During peak periods, the HP system is turned off and the thermal battery is activated to meet the required building load through the hydronic loop, thereby expected to reduce overall electricity usage. Once the PCM is fully depleted, the base HP system is utilized to meet the building load while the PCM is recharged.

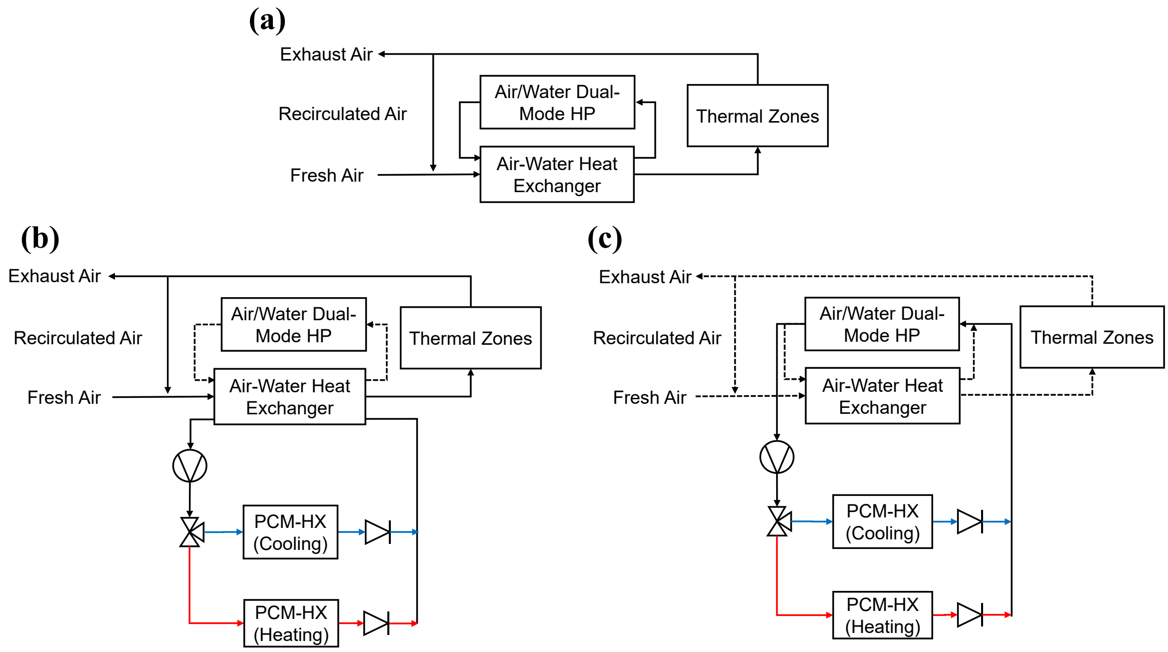

Figure 2. HP-TES system schematic diagrams: (a) base operation, (b) discharge operation, (c) recharge operation

The base system consists of an air-to-water heat pump equipped with an outdoor microchannel coil, a single-speed compressor, and a braze plate heat exchanger (BPHX), connecting to the indoor air-to-water coil in discharge mode or to the PCM-HXs during TES recharge. In cooling mode, the BPHX solidifies the PCM, while in heating mode, it melts the PCM. A 45% propylene glycol/water mixture is used as the heat transfer fluid in the hydronic loop to provide freeze protection, particularly during heating season charging events when evaporating temperatures fall below freezing. The refrigerant R410A is used for heat pump operation in both heating and cooling modes.

2.3. Modelica Interface and Performance Maps Integration with Spawn of EnergyPlus™

Figure 3 shows the Dymola interface of the HP-TES system incorporating the PCM-HX performance maps, Spawn of EnergyPlus™ [15], and the DOE small office prototype [13]. A rule-based control logic was developed to flexibly switch between providing space conditioning using the base HP and TES discharge and recharge. For example, HP-TES integrations in literature have considered control strategies where TES is only used during the location-specific utility peak time of use (TOU) hours or according to model-predictive control frameworks based on PCM state-of-charge (SOC) [26]. In this study, the HP-TES control strategies were developed according to the TOU schedule for Vienna, Austria, following the KELAG electricity tariff, which remains constant throughout the year and defines on-peak periods from 6:00 to 9:00 and 16:00 to 22:00 [27].

The HP-TES controller requires two external inputs: the daily operating hours (i.e., TOU hours), to determine when TES discharge or recharge is enabled, and the thermostat setpoints, which regulates indoor temperature via HVAC (de)activation in response to building thermal loads. Discharge occurs during on-peak periods when the PCM SOC is between 95% to 5%. Once the liquid fraction drops below 5%, the control signal shifts the operation to recharge, which occurs during off-peak (night-time) periods to minimize energy consumption, i.e., the coolest night-time hours for cooling mode (latest nocturnal hours) and the warmest for heating (earliest nocturnal hours). During recharge, the final liquid fraction from the discharge cycle is used as the initial condition. Once the recharge is completed (SOC ≥ 95%), the system resets, and the discharge mode is possible for the next TOU cycle.

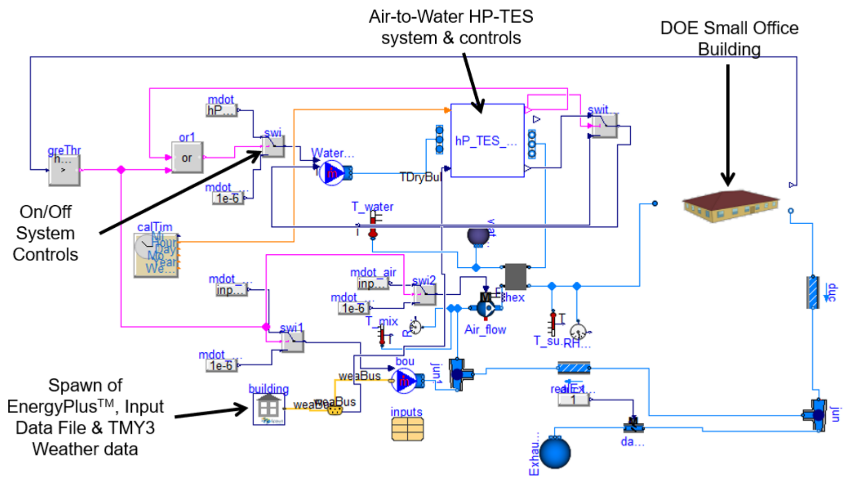

Figure 3. Dymola interface of HP-TES system, DOE small office prototype building, and Spawn of EnergyPlus™

3. Results and Discussion

3.1. PCM-HX Performance Prediction

The TES performance was first predicted using GRCM, and the outputs were employed to construct the PCM-HX performance maps in both heating and cooling modes under fixed inlet HTF temperature and constant thermal battery mass flow rate of 0.78 kg/s. Fitted UA coefficient values were used to define the discharge and recharge processes in both cooling and heating modes (Table 2).

Table 2. UA coefficients for PCM-HX cooling and heating mode performance maps

Coefficient	Cooling Mode (A12)		Cooling Mode (A16)		Heating Mode (A31)		Heating Mode (A36)	
	Discharge	Recharge	Discharge	Recharge	Discharge	Recharge	Discharge	Recharge
C_1	8.7E+03	3.8E+02	8.8E+03	3.8E+02	4.1E+02	8.0E+03	4.1E+02	8.0E+03
C_2	-2.0E+04	1.5E+04	-2.1E+04	1.5E+04	1.5E+04	-1.5E+04	1.6E+04	-1.6E+04
C_3	5.1E+04	-3.1E+04	5.2E+04	-3.1E+04	-3.0E+04	3.8E+04	-3.0E+04	3.9E+04
C_4	-8.4E+04	5.3E+04	-8.6E+04	5.3E+04	4.6E+04	-6.4E+04	4.7E+04	-6.7E+04
C_5	7.0E+04	-5.2E+04	7.3E+04	-5.3E+04	-4.2E+04	5.4E+04	-4.3E+04	5.7E+04
C_6	-2.5E+04	2.3E+04	-2.6E+04	2.4E+04	1.8E+04	-2.0E+04	1.9E+04	-2.1E+04

Figure 4 presents a comparison of the full GRCM prediction and the performance map-based PCM-HX component model simulated in Modelica, highlighting the heat transfer rate vs. liquid fraction for all four operating modes. Overall, there is good agreement between the Modelica performance map-based PCM-HX component and GRCM, with an average absolute percentage error ranging from 2.3% to 3.6%, and maximum percentage error of 10.9% during shut-down of cooling mode recharge. The discrepancy between the two models is likely due to the curve-fit being less accurate during start-up and shut-down operations, as the performance maps methodology was developed to represent the phase-change process only. Nevertheless, the performance maps model successfully reproduces the TES behavior inside Modelica, showing good prediction overall. The root mean square error (RMSE) between the two curves ranges from 0.3 to 0.5, with maximum value of 1.0 for heat transfer prediction during cooling mode recharge. A key advantage of employing the proposed performance map methodology lies in the considerable reduction in simulation time. The performance map-based PCM-HX in Modelica was found to be at least 1800 times faster compared to full

GRCM simulations, providing the computational speed increase necessary for coupling with large-scale building energy and control simulations over a full year without compromising component-level accuracy.

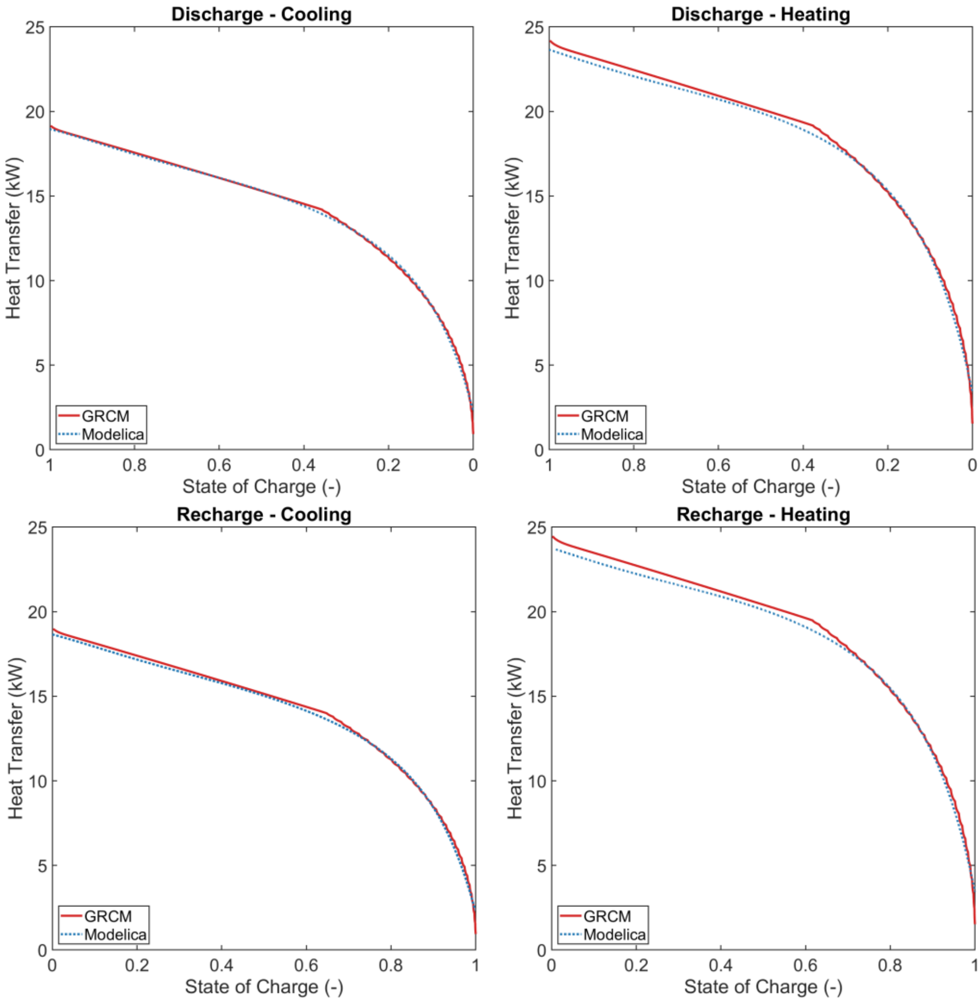

Figure 4. Modelica PCM-HX curve-fit model verification vs. full GRCM simulation

3.2. Daily HP-TES System Level Simulation

Daily simulations were conducted using HP-TES performance maps to ensure that the methodology can enable system-level performance assessment. The simulations were carried out over a typical meteorological day (midnight to midnight) for Jan 8th (heating mode) and Jun 28th (cooling mode) in Vienna, Austria. During TOU hours (6:00 to 9:00 and 16:00 to 22:00), the system shifts from base HP to TES discharge until the PCM is fully depleted, then switches to base HP space conditioning and TES recharge during off-peak periods, thereby mitigating peak electricity demand.

3.2.1. Heating Mode

Figure 5 illustrates the base HP operation, showing the compressor power consumption, outdoor air temperature, and indoor thermostat setpoint temperature of 20°C ± 1 K. The cold and dry climate conditions in Vienna, Austria, result in continuous compressor operation throughout the winter day (Jan 8th) to meet the heating demand. Figure 6 presents the full-day winter simulation for HP-TES operation, comparing two PCMs with different melting temperatures (A31 and A36) in terms of power consumption and discharge capacity. The PCM with the higher melting temperature (A36) achieved greater demand reduction and maintained system operation for a longer duration during peak hours. However, due to its higher melting temperature, A36 required a longer and more energy-intensive recharge period than A31, attributed to the increased system temperature lift. Despite the higher compressor power with A36, the total on-peak energy savings reached 38.7%, compared to 34% for A31.

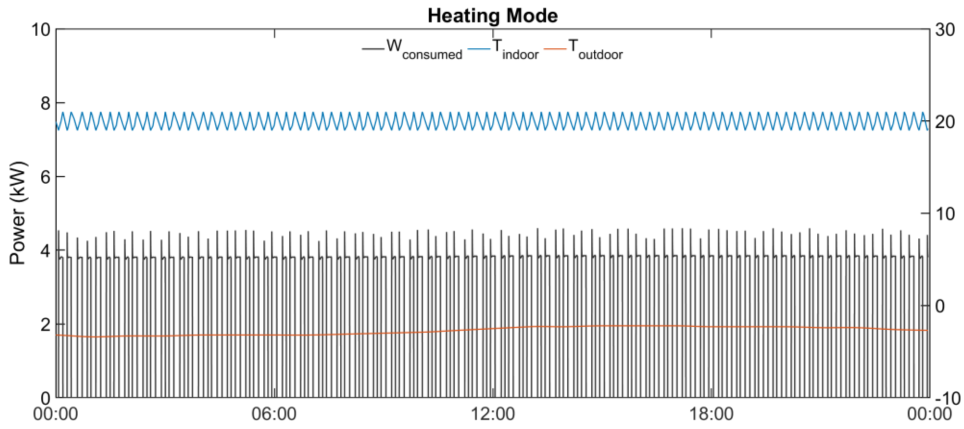

Figure 5. Base heat pump operation during heating mode

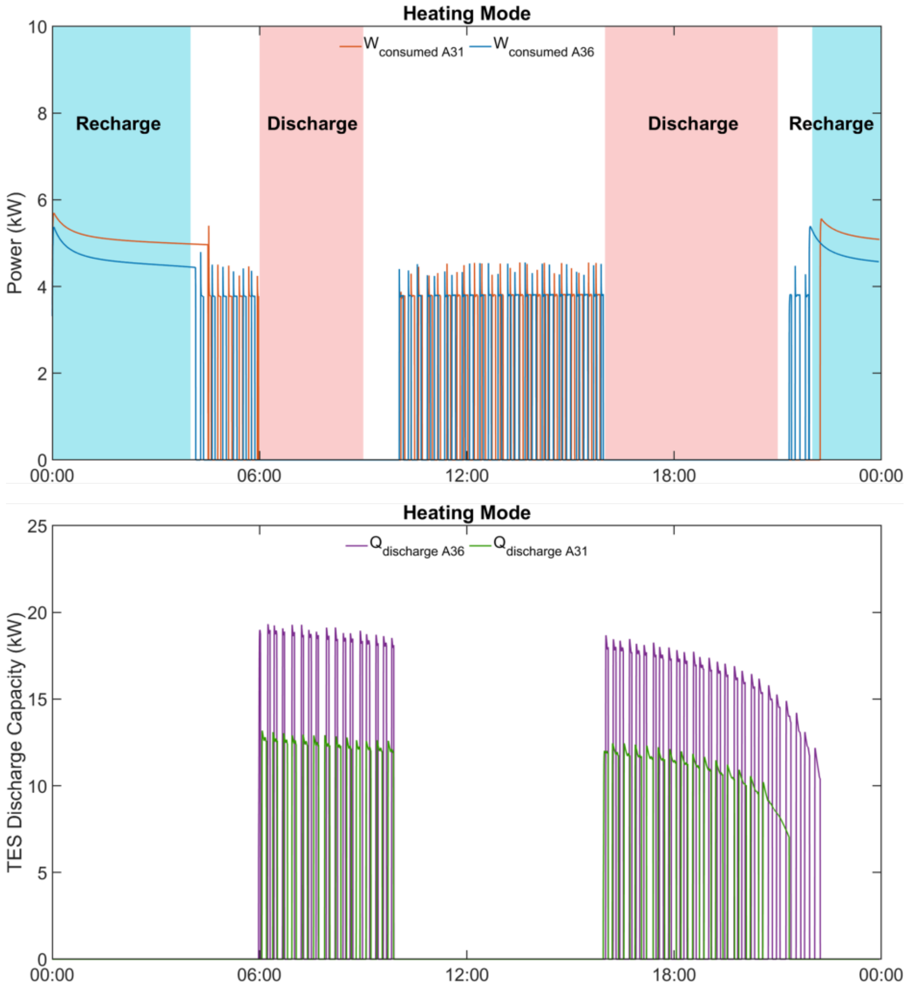

Figure 6. Compressor power consumption (top) and TES heat load (bottom) using PCMs A31 and A36

3.2.2. Cooling Mode

Since Vienna, Austria, has a heating-dominant climate, the operating of base HP operation during the representative summer day (Jun 28th) was less frequently than the representative winter day (Jan 8th), Figure 7. During night-time the outdoor air temperature remained below the indoor thermostat setpoint (24°C ± 1 K), resulting in no cooling demand and consequently no HP activation. The unit begins operating only during daytime, maintaining indoor temperature stable through intermittent compressor cycling. In addition, Figure 8 shows the compressor power consumption and the discharge capacity from the HP-TES unit. The HP remains inactive during the early morning and late evening hours when the ambient temperature is below the indoor setpoint, similar to the base case. Both A12 and A16 exhibit comparable power and profiles during active periods, indicating similar compressor cycling behavior. Although A12 provides a higher discharge capacity than A16, both systems achieve comparable on-peak energy savings since they operate over nearly the same discharge period during peak demand. The total on-peak energy savings are approximately 34.3% for A12 and 32.0% for A16.

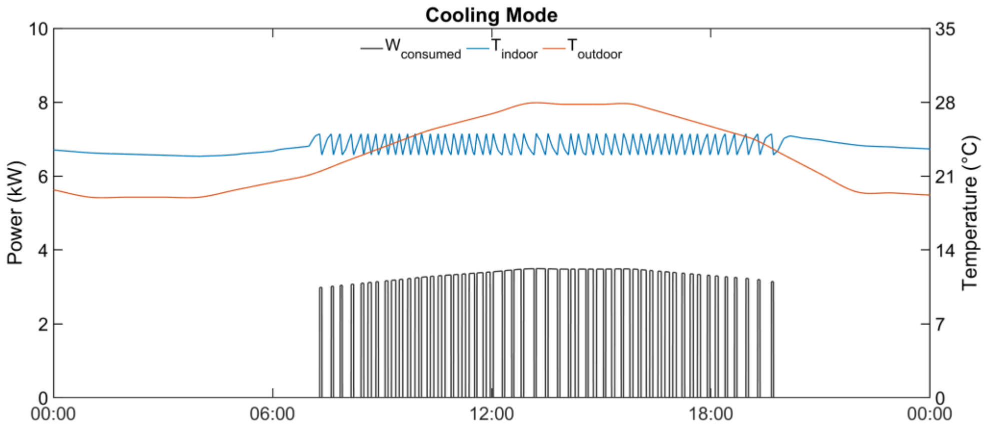

Figure 7. Base heat pump operation during cooling mode

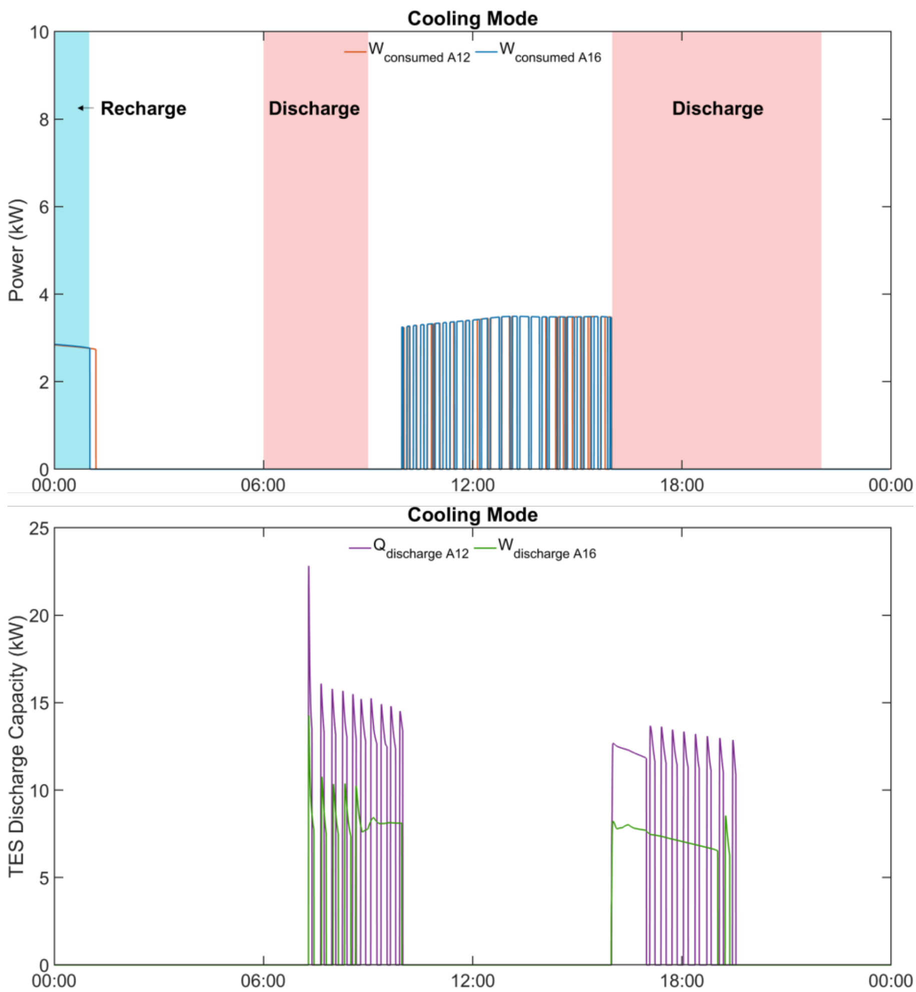

Figure 8. Compressor power consumption (top) and TES cooling load (bottom) using PCMs A12 and A16

4. Conclusion

This paper presents a computationally efficient framework for simulating building energy systems integrated with LHTES. In this approach, PCM-HXs are represented using performance maps constructed using source data from a generalized RC modeling tool, which are then integrated into HP system models as curve-fit components and simulated in Modelica with building loads computed using Spawn of EnergyPlus™ to determine the impact of HP-TES systems on building energy consumption. The performance maps showed excellent when implemented as a dynamic component model in Modelica, characterizing the PCM-HX behavior with excellent accuracy while achieving at least 10^3 computational time reduction compared to full GRCM simulations. The performance map methodology was further verified by considering daily simulation in cooling and heating modes in Vienna, Austria. Since Vienna is a heating-dominant climate, it was found that PCMs with high melting temperature can result in more energy savings (39%) due to peak demand savings resulting from higher temperature lifts. On the other hand, PCM-TES recharge process is considerably more energy-intensive. For cooling mode, different PCM melting temperature had minimal impact, presenting almost the same on-peak energy savings. Overall, the proposed performance maps methodology provides a robust and accurate modeling framework for PCM-HXs in a component and system level integration, opening new opportunities for advanced control strategy development and parametric analysis of TES configurations in a computationally efficient manner.

Acknowledgements

This material is based upon work supported by the U.S. Department of Energy's Office of Energy Efficiency and Renewable Energy (EERE) under the Building Technologies Office (BTO) Award Number DE-EE0009158. The views expressed herein do not necessarily represent the views of the U.S. Department of Energy or the United States Government. This work was also supported in part by the Modeling & Optimization Consortium at the Center for Environmental Energy Engineering at the University of Maryland.

Nomenclature

BPHX	Brazed Plate Heat Exchanger	(–)	TOU	Time of use	(–)
c_p	Specific heat	(kJ/kgK)	UA	Thermal Conductance	(W/K)
H	Latent Heat	(kJ/kg)	Δ	Variation	(–)
HP	Heat Pump	(–)	V	Volume	(m^3)
HX	Heat Exchanger	(–)	ρ	Density	(kg/m^3)
GRCM	Generalized Resistance-Capacitance Model	(–)	x	Liquid fraction	(–)
LMTD	Log mean temperature difference	(K)	**Subscript**		
PCM	Phase Change Material	(–)	CF	Curve-fit	(–)
Q	Heat rate	(kW)	i	initial	(–)
SOC	State of charge	(–)	f	final	(–)
t	time	(s, h)	melt	melting	(–)
TES	Thermal Energy Storage	(–)	sol	solidification	(–)

References

[1] S. Anweiler *et al.*, "Performance Variability of Air-Water Heat Pumps in Cold and Warm Years Across European Climate Zones," 2025, *SSRN*. doi: 10.2139/ssrn.5087259.

[2] European Heat Pump Association (EHPA), "European Heat Pump Market Report." Accessed: Nov. 03, 2025. [Online]. Available: https://ehpa.org/market-data/#:%7E:text=2.18%20million%20heat%20pump%20units,of%20the%20heating%20market

[3] Ç. Yıldız, M. Arıcı, M. Seçilmiş, and D. Li, "Experimental and numerical assessment of thermal energy storage unit with PCM integrated to air source heat pump for enhancement of load shifting," *Energy Convers. Manag.*, vol. 345, p. 120342, Dec. 2025, doi: 10.1016/j.enconman.2025.120342.

[4] H. Togun *et al.*, "A critical review on phase change materials (PCM) based heat exchanger: Different hybrid techniques for the enhancement," *J. Energy Storage*, vol. 79, p. 109840, Feb. 2024, doi: 10.1016/j.est.2023.109840.

[5] R. A. Kishore, M. V. A. Bianchi, C. Booten, J. Vidal, and R. Jackson, "Optimizing PCM-integrated walls for potential energy savings in U.S. Buildings," *Energy Build.*, vol. 226, p. 110355, Nov. 2020, doi: 10.1016/j.enbuild.2020.110355.

[6] V. Piroozmand and R. Ahmadi, “Enhancement of PCMs performance using nano-particles in horizontal triple-series shell-and-tube heat exchangers: A numerical study,” *J. Energy Storage*, vol. 85, no. December 2023, p. 111057, 2024, doi: 10.1016/j.est.2024.111057.

[7] Y. Li, Z. O’Neill, L. Zhang, J. Chen, P. Im, and J. DeGraw, “Grey-box modeling and application for building energy simulations - A critical review,” *Renew. Sustain. Energy Rev.*, vol. 146, p. 111174, Aug. 2021, doi: 10.1016/j.rser.2021.111174.

[8] T. Alam, D. Bacellar, J. Ling, and V. Aute, “Development and Validation of Resistance-Capacitance Model for Phase Change Material Embedded in Porous Media,” *Intersoc. Conf. Therm. Thermomechanical Phenom. Electron. Syst. ITHERM*, vol. 2022-May, no. 2011, pp. 1–10, 2022, doi: 10.1109/iTherm54085.2022.9899532.

[9] M. Menezes, J. Tancabel, D. Bacellar, and V. Aute, “Development & Experimental Validation of a Generalized Resistance-Capacitance Model for Numerical Simulation of Phase-Change Material Embedded Heat Exchangers,” *20th Int. Refrig. Air Cond. Conf.*, pp. 1–10, 2024.

[10] R. Kamal, F. Moloney, C. Wickramaratne, A. Narasimhan, and D. Y. Goswami, “Strategic control and cost optimization of thermal energy storage in buildings using EnergyPlus,” *Appl. Energy*, vol. 246, pp. 77–90, July 2019, doi: 10.1016/j.apenergy.2019.04.017.

[11] J. Marchante-Avellaneda, E. Navarro-Peris, and Y. Song, “Development of map-based models for the performance characterization in a new prototype of Dual Source Heat Pump,” *Appl. Therm. Eng.*, vol. 236, p. 121743, Jan. 2024, doi: 10.1016/j.applthermaleng.2023.121743.

[12] P. Ihm, M. Krarti, and G. P. Henze, “Development of a thermal energy storage model for EnergyPlus,” *Energy Build.*, vol. 36, no. 8, pp. 807–814, Aug. 2004, doi: 10.1016/j.enbuild.2004.01.021.

[13] Dept. of Energy Building Technologies Office, “Prototype Building Models | Building Energy Codes Program,” 2022, Accessed: Nov. 03, 2022. [Online]. Available: https://www.energycodes.gov/prototype-building-models

[14] “ASHRAE International Weather Files for Energy Calculations 2.0 (IWEC2).” Accessed: Nov. 01, 2025. [Online]. Available: https://www.ashrae.org/technical-resources/bookstore/ashrae-international-weather-files-for-energy-calculations-2-0-iwec2

[15] M. Wetter, K. Benne, H. Tummescheit, and C. Winther, “Spawn: coupling Modelica Buildings Library and EnergyPlus to enable new energy system and control applications,” *J. Build. Perform. Simul.*, vol. 17, no. 2, pp. 274–292, Mar. 2024, doi: 10.1080/19401493.2023.2266414.

[16] M. Wetter, W. Zuo, T. S. Nouidui, and X. Pang, “Modelica Buildings library,” *J. Build. Perform. Simul.*, vol. 7, no. 4, pp. 253–270, July 2014, doi: 10.1080/19401493.2013.765506.

[17] https://www.3ds.com/products/catia/dymola, *Dymola*. Modelica. Dassault Systèmes.

[18] “Standard 90.1.” Accessed: June 29, 2025. [Online]. Available: https://www.ashrae.org/technical-resources/bookstore/standard-90-1

[19] Air-conditioning, Heating & Refrigeration Institute (AHRI), “Performance Rating of Unitary Air-conditioning and Air-source Heat Pump Equipment,” Standard 210/240, 2024. [Online]. Available: https://www.ahrinet.org/search-standards/ahri-210240-i-p-performance-rating-unitary-air-conditioning-and-air-source-heat-pump-equipment

[20] “PlusICE Range 2021-1 - PCM Products Ltd.”

[21] Dion King and Robert Potter, “Description of Steady-State Cooling Plant Model Developed for Use in Evaluating Optimal Control of Ice Thermal Storage Systems,” *ASHRAE Trans. 1998*, vol. 104, p. 12, Oct. 1998.

[22] Gregor P. Henze and Moncef Krarti, “Predictive Optimal Control of Active and Passive Building Thermal Storage Inventory,” University of Nebraska, DE-FC-26-01NT41255, Sept. 2001.

[23] H. Qiao, V. Aute, and R. Radermacher, “Transient modeling of a flash tank vapor injection heat pump system – Part I: Model development,” *Int. J. Refrig.*, vol. 49, pp. 169–182, Jan. 2015, doi: 10.1016/j.ijrefrig.2014.06.019.

[24] A.-H. Othman, V. Aute, and J. Tancabel, “Recharge Demand Mitigation for Latent Heat Thermal Energy Storage at Off-peak Hours,” in *8th International High-Performance Buildings Conference*, 2024.

[25] A.-H. Othman, V. Aute, and J. Tancabel, “Performance Assessment of a Dual-purpose HP-TES for a Typical Year Comparing Different Climate Zones,” 2024.

[26] Z. Shen, D. Howard, D. Hun, S. Mumme, and S. Shrestha, “Coupling thermal energy storage with a thermally anisotropic building envelope for building demand-side management across various US climate conditions,” *Energy Build.*, vol. 328, p. 115204, Feb. 2025, doi: 10.1016/j.enbuild.2024.115204.

[27] N. Houben *et al.*, “Optimal dispatch of a multi-energy system microgrid under uncertainty: A renewable energy community in Austria,” *Appl. Energy*, vol. 337, p. 120913, May 2023, doi: 10.1016/j.apenergy.2023.120913.